

Electronic Supplementary Information (ESI)

## **Insights into the Excitonic Processes in Polymeric Photocatalysts†**

Hui Wang,<sup>‡</sup> Shenlong Jiang,<sup>‡</sup> Shichuan Chen, Xiaodong Zhang\*, Wei Shao, Xianshun Sun, Zhi Zhao, Qun Zhang\*, Yi Luo and Yi Xie\*

Hefei National Laboratory for Physical Science at Microscale, Collaborative Innovation Center of Chemistry for Energy Materials, Synergetic Innovation Center of Quantum Information and Quantum Physics, University of Science and Technology of China, Hefei, Anhui, 230026, P. R. China

Email: zhxid@ustc.edu.cn, qunzh@ustc.edu.cn, yxie@ustc.edu.cn

## Experimental section

**Preparation of graphitic carbon nitride.** The g-C<sub>3</sub>N<sub>4</sub> sample was prepared by thermal condensation of melamine molecules. In detail, 20 g of melamine was put into a crucible (30 ml) with a cover and kept at 600 °C for 10 h in a tube furnace with a ramp rate of ~5°C/min for both the heating and cooling processes. After being cooled down, the obtained yellow product was collected and washed with distilled water to remove residual ammonium. The sample was then dried and stored under dark condition for further characterizations.

**Characterization methods.** The X-ray diffraction (XRD) measurements were carried out on a Philips X'Pert Pro Super diffractometer with Cu K $\alpha$  radiation ( $\lambda = 1.54178$  Å). The X-ray photoelectron spectra (XPS) were recorded on an ESCALAB MKII with Mg K $\alpha$  ( $h\nu = 1253.6$  eV) as the excitation source. The binding energies derived from the XPS analysis were corrected against the specimen charging by referencing C 1s to 284.8 eV. The Ultraviolet–visible (UV–Vis) spectra were obtained on a Perkin Elmer Lambda 950 UV–vis–NIR spectrophotometer. The Fourier transform infrared (FT-IR) spectra were recorded on a Magna-IR750 FT-IR spectrometer in a KBr pellet, scanning from 4000 to 400 cm<sup>-1</sup> at room temperature. The steady-state and time-resolved phosphorescence spectra were obtained on a FLUOROLOG-3-TAU fluorescence spectrometer (Jobin Yvon Ltd.). The steady-state and time-resolved fluorescence spectra were obtained on an FLS920 fluorescence spectrometer (Edinburgh Instruments Ltd.). Time-resolved fluorescence spectra were recorded with 365 nm excitation, while other spectra were obtained with 400 nm excitation. All steady-state phosphorescence spectra were recorded by accumulating 10 flash counts per point.

**Hydrogen evolution measurements.** 20 mg of catalyst powders was dispersed in the aqueous solution (200 mL) containing methanol (18 vol.%) and ethanol/2-bromoethanol (2 vol.%). Before test, the reaction solution was evacuated several times to remove air completely prior to irradiation under a 300W Xe-lamp (PLS-SXE300/300UV, Trusttech Co., Ltd., Beijing).

**ESR measurements.** 50  $\mu\text{L}$  of aqueous suspension of samples ( $4 \text{ g L}^{-1}$ ) was mixed with 500  $\mu\text{L}$  of 2,2,6,6-tetramethylpiperidine (TEMP, 50 mM) aqueous solution containing ethanol/2-bromoethanol (20 vol.%). After being illuminated for 30 seconds, the mixture was characterized using a Bruker EMX plus model spectrometer operating at the X-band frequency (9.4 GHz) at room temperature. The control  $\text{O}_2^{\cdot -}$  trapping-ESR tests were also performed as described above, except the use of 5,5-dimethyl-1-pyrroline-N-oxide (DMPO, 20 mM) as the spin-trapping agent. A xenon lamp (50 W) with a 380-nm cutoff filter was used as light source. Note that the catalysts used in ESR-trapping tests do not contain metal Pt or any other co-catalyst.

**Ultrafast transient absorption (TA) spectroscopy characterizations:** The femtosecond transient absorption data were recorded on a modified pump–probe spectrometer (ExciPro, CDP) in combination with an ultrafast amplified laser system. The pump pulses (centre wavelength at 400 nm used in this work; pulse energy  $\sim 5 \mu\text{J}$  at the sample cell) were delivered by an optical parametric amplifier (TOPAS-800-fs, Coherent), which was excited by a Ti:sapphire regenerative amplifier (Legend Elite-1K-HE, Coherent; centre wavelength  $\sim 800 \text{ nm}$ , pulse duration  $\sim 25 \text{ fs}$ , pulse energy  $\sim 3 \text{ mJ}$ ) seeded with a mode-locked Ti:sapphire laser system (Micra 5, Coherent) and pumped with a 1-kHz Nd:YLF laser (Evolution 30, Coherent). The much weaker probe pulses were provided by a stable white-light continuum (WLC; 420–720 nm monitored in this work) that was generated by focusing the 800-nm beam (split from the regenerative amplifier by a portion of  $\sim 10\%$ ) in a rotating 4.55-mm-thick  $\text{CaF}_2$  crystal. The linear chirp of the WLC spectrum was compensated with the aid of the cross-phase modulation signals recorded on a liquid hexane sample using an ExiPro 2.6 software. The WLC pulse was free of pre-pulsing and after-pulsing, as verified by our routine pulse characterizations. The pump and probe beams were collinearly polarized. The instrument response function was determined to be  $\sim 80 \text{ fs}$  by cross-correlating the pump and probe pulses at the sample cell. Precise spatial overlap of the pump and probe beams (with diameters of  $\sim 1500$  and  $\sim 300 \mu\text{m}$ , respectively) at the centre of the 1.2-mm-thick sample cell (quartz) was attained by optimizing the transient absorption signals with the aid of a laser beam analyzer

(BG-USB-SP620, Ophir-Spiricon). The time delay between the pump and probe pulses (i.e., probe delay, in short) was varied by a motorized optical delay line (minimum step 1.56 fs; maximum delay ~3 ns). The time zero of probe delay was determined by cross-correlating the pump and probe pulses at the sample cell *in situ* and also carefully cross-checked with other chemical samples such as the DCM and LDS698 dyes. A mechanical chopper operating at 500 Hz was utilized to modulate the pump pulses such that the transient absorption spectra with and without the pump pulses can be recorded alternately. The WLC probe beam was first split into two tiny portions to synchronize the chopper and monitor the stability of the probe pulses using two separate photodiode detectors, and then separated into two parts (~70/30 in percentage), with the 70% part focused on the sample cell and overlapped with the pump beam yielding a transmitted probe signal, while the 30% part focused onto another place of the sample cell to serve as a reference signal for achieving a best signal-to-noise ratio. The sample cell containing the colloidal samples under investigation was mounted on a rapidly rotating stage (5000 rpm) so as to ensure that the photoexcited volume of the sample was kept fresh during the course of the pump–probe measurements. The temporal and spectral profiles of the transient absorption signal, i.e., the pump-induced transient absorbance changes (in mOD; OD, optical density) were visualized by a 1024-pixel imaging spectrometer (CDP2022i) and further processed with the ExiPro 2.6 software equipped with the pump–probe system.

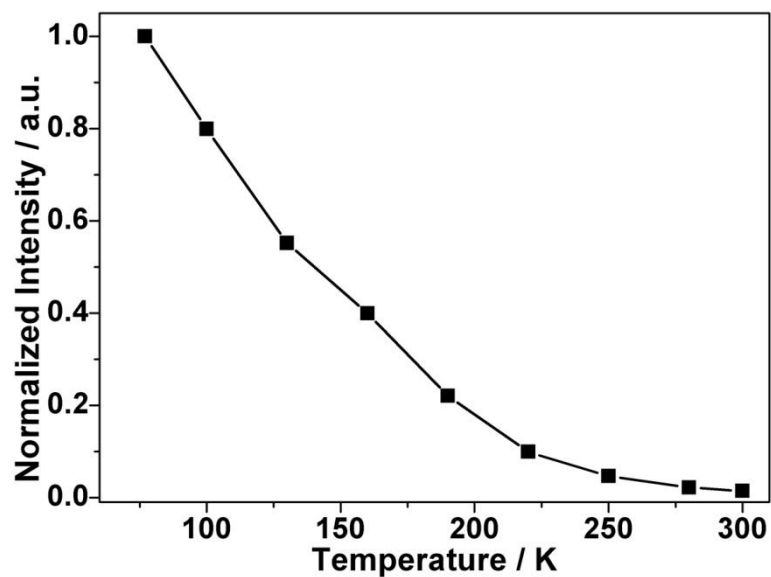


**Fig. S1** Temperature-dependent fluorescent intensity measured with excitation at 365 nm and emission at 450 nm, which increases with decreasing temperature.

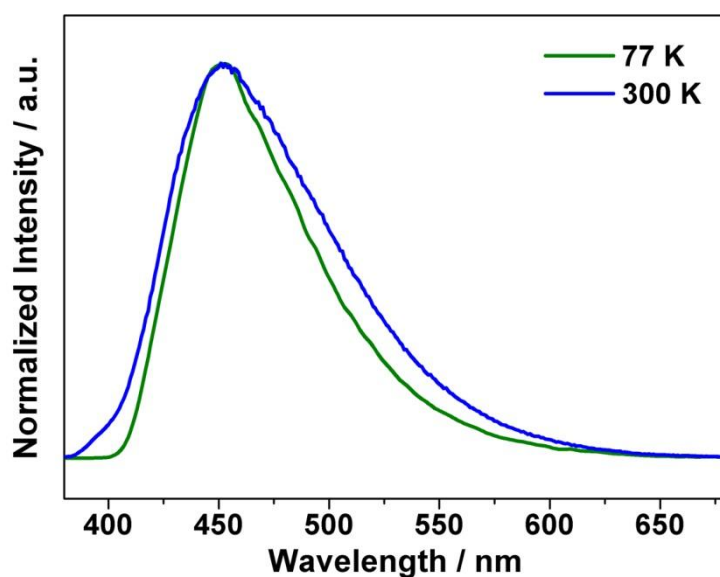


**Fig. S2** Prompt fluorescence spectra under 77 and 300 K, respectively. The 77 K-case exhibits narrowed prompt emission towards 300 K-case, suggesting the promoted contribution of singlet-exciton radiative recombination towards prompt fluorescence.

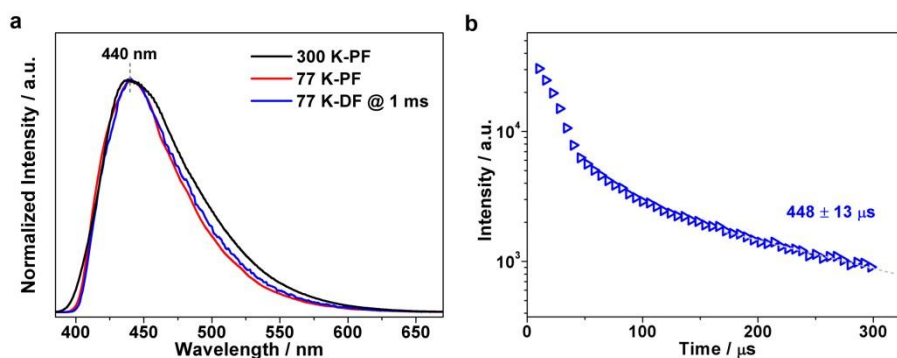


**Fig. S3** (a) Normalized photoluminescence spectra under 77 and 300 K (PF: prompt fluorescence; DF: delayed fluorescence). (b) Time-resolved DF kinetics monitored at the emission peak at 77 K.

As is known, graphitic carbon nitride (strictly speaking, polymeric heptazine-based melon) contains abundant  $\text{-NH}_2$  groups and other defects that are inevitably generated during thermal condensation process, which undoubtedly impact the properties of samples. In this regard, it would be quite necessary to gain an in-depth understanding on the influence of these defective structures toward excitonic process in carbon nitride matrix.

To address this issue, we took oxidized carbon nitride (CNO, Ref. [18]) as an example to interrogate the influence of structural defects on excitonic effects. According to our previous work, the amine groups have been removed through the oxidation treatment, but with the incorporation of carbonyl groups (some kind of defective structure on carbon nitride matrix). As shown in **Fig. S3a**, the CNO sample still possesses pronounced delayed fluorescence (DF) under low temperatures. In detail, the prompt fluorescence (PF) obtained at 77 K exhibits narrowed emission with respect to the 300-K case, suggesting the promoted contribution of singlet-exciton radiative recombination. Meanwhile, the steady-state phosphorescence emission monitored at 1 ms turned out to be nearly identical to the PF profile under 77 K, suggesting the DF feature caused by the robust triplet-triplet annihilation in the oxidized polymer matrix. These results clearly indicate that the strong correlations (e.g., excitonic effects, triplet-triplet annihilation) among the photogenerated species are not dependent on these defective structures. On the other hand, the blue-shifted PF

emission with respect to the pristine counterpart is certainly related to the structural changes through oxidation treatment. Moreover, the time-resolved DF kinetics monitored at 440 nm yields a lifetime of  $\sim 448 \mu\text{s}$  (**Fig. S3b**). The accelerated DF relaxation is ascribed to the promoted ISC process due to the introduction of carbonyl groups. These emission features clearly rely on these defects.

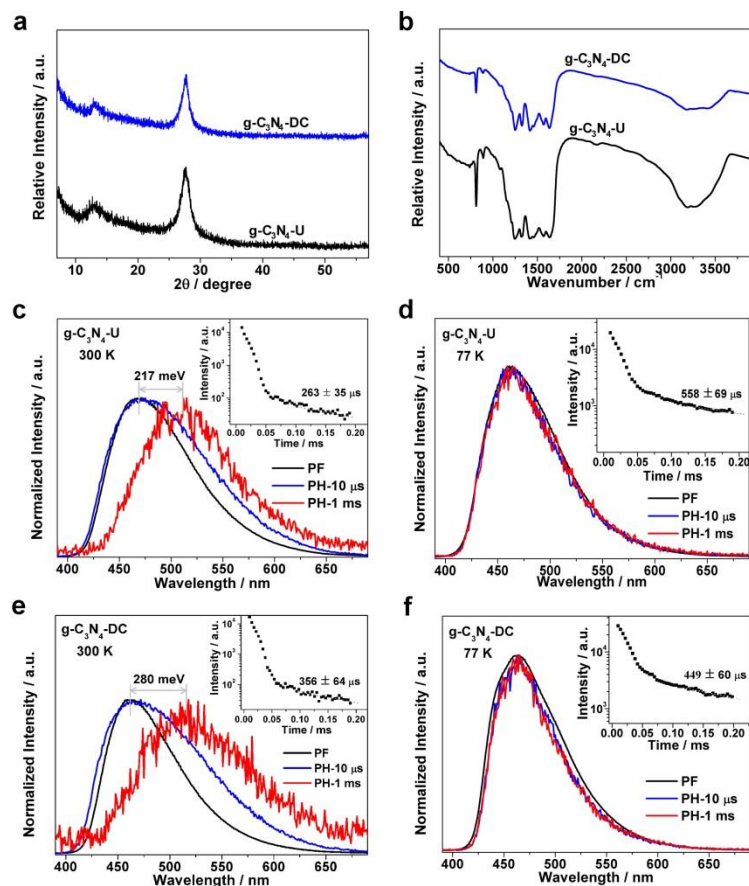


**Fig. S4** (a) XRD patterns and (b) FT-IR spectra of  $g\text{-C}_3\text{N}_4\text{-U}$  and  $g\text{-C}_3\text{N}_4\text{-DC}$ , respectively. (c) and (d) normalized steady-state PF and PH spectra of  $g\text{-C}_3\text{N}_4\text{-U}$  recorded at 300 K and 77 K. (e) and (f) normalized steady-state PF and PH spectra of  $g\text{-C}_3\text{N}_4\text{-DC}$  recorded at 300 K and 77 K. Inset: corresponding time-resolved PH kinetics.

Given the ill-defined crystal structure of polymeric carbon nitride, we are inspired to investigate the excitonic processes of some other samples obtained under other conditions as comparison. Herein, urea and dicyandiamide were employed as the precursors for preparing different carbon nitrides, with products denoted as  $g\text{-C}_3\text{N}_4\text{-U}$  and  $g\text{-C}_3\text{N}_4\text{-DC}$ , respectively. Structural characterizations (XRD and FT-IR, as shown in **Fig. S4a** and **S4b**) of the samples suggested that carbon nitride with tri-s-triazine-based structure have been successfully obtained by the thermal condensation of different precursors. To go further, photoluminescence measurements were carried out to interrogate the excitonic processes in  $g\text{-C}_3\text{N}_4\text{-U}$  and  $g\text{-C}_3\text{N}_4\text{-DC}$ .

As shown in **Fig. S4c** (**Fig. S4e**), prompt fluorescence and phosphorescence spectra recorded at 300 K were found to peak at 469 (462) and 511 (516) nm for g-C<sub>3</sub>N<sub>4</sub>-U (g-C<sub>3</sub>N<sub>4</sub>-DC), suggesting a singlet–triplet energy gap of ~0.217 (~0.280) eV. These significant differences confirm that carbon nitride matrixes obtained from different precursors possess obviously different singlet and triplet states energy levels, even with almost same structural characterization results. On the other hand, the 10- $\mu$ s delayed emissions of the two samples nearly coincide with their PF profiles but the wings to the red are broadened, which could be attributed to delayed fluorescence. Moreover, low-temperature measurements (**Fig. S4d** and **S4f**) suggest that the steady-state emissions monitored at 10  $\mu$ s and 1 ms turn out to be nearly identical to corresponding PF profiles, confirming the P-type delayed fluorescence originates from the robust triplet–triplet annihilation (TTA) process in the two samples. In that case, it would be safe to conclude the inherent properties of excitonic effects and triplet–triplet annihilation in carbon nitride matrix.

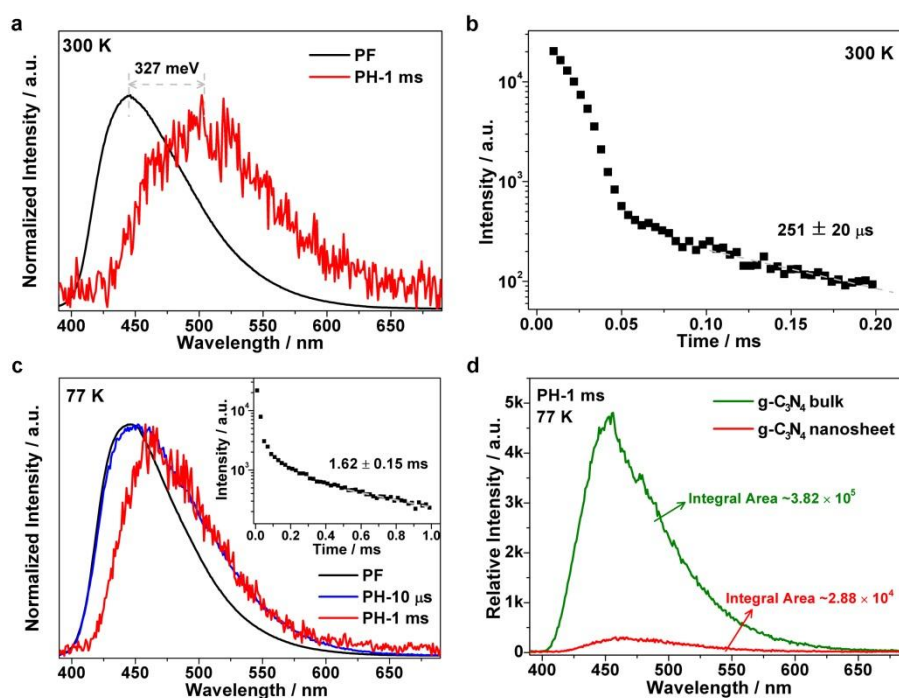


**Fig. S5** (a) Normalized steady-state PF and PH spectra at 300 K (delay time 1 ms), (b) time-resolved PH kinetics at 300 K, and (c) normalized steady-state PF and PH spectra at 77 K (Inset: corresponding time-resolved PH kinetics) of g-C<sub>3</sub>N<sub>4</sub> nanosheets. (d) Steady-state PH spectra (delay time 1 ms) of g-C<sub>3</sub>N<sub>4</sub> bulk and nanosheets at 77 K.

The dimension of g-C<sub>3</sub>N<sub>4</sub> has great influence on the photoexcitation processes, giving rise to enormous intriguing optical properties.<sup>1–4</sup> To identify the influence of thickness on excitonic process in carbon nitride matrix, we here interrogate the photoluminescence properties of carbon nitride nanosheets. Herein, carbon nitride nanosheets were obtained through liquid-phase exfoliation in water.<sup>1</sup> Steady-state prompt fluorescence (PF) and phosphorescence (PH) spectra of carbon nitride nanosheets recorded at 300 K give a singlet–triplet energy gap ( $\Delta E_{ST}$ ) of  $\sim 0.327$  eV (**Fig. S5a**). The much larger  $\Delta E_{ST}$  (with respect to the bulk one, 0.243 eV) appeal a potential adverse effect on intersystem crossing (ISC) process, thus giving faint triplet exciton generation.<sup>5,6</sup> In addition, the enhanced conjugation in the nanosheet matrix would possess much weak spin–orbit coupling, which also suppresses ISC efficiency.

Time-resolved PH spectrum gives a triplet lifetime of  $\sim 251 \mu\text{s}$  (**Fig. S5b**), which might imply the potential weak correlations among excitons. To this end, low-temperature photoluminescence measurements were further performed. As shown in **Fig. S5c**, the slight red-shifted PH spectra (with respect to PF spectra, but not exact emission of triplet exciton) suggest the faint delayed fluorescence feature in carbon nitride nanosheet. Moreover, the  $\sim 1.62 \text{ ms}$  lifetime further confirmed the reduced triplet–triplet annihilation in low-dimensional carbon nitride matrix, with respect to bulk ones.

According to previous reports,<sup>7,8</sup> intersystem crossing efficiency ratio of carbon nitride nanosheets versus bulk counterpart would be written as

$$\left(\frac{\Phi_{\text{nanosheet}}}{\Phi_{\text{bulk}}}\right)^2 = \left(\frac{I_{\text{nanosheet}}}{I_{\text{bulk}}}\right) \left(\frac{\varphi_{\text{nanosheet}}}{\varphi_{\text{bulk}}}\right)^{-1} \left(\frac{\tau_{\text{nanosheet}}}{\tau_{\text{bulk}}}\right)^{-2}$$

where  $I$  is the DF intensity ( $2.88 \times 10^4$  vs.  $3.82 \times 10^5$ , **Fig. S5d**),  $\tau$  the lifetime of the triplet (which is equal to twice the lifetime of DF,  $3.24 \text{ ms}$  vs.  $1.59 \text{ ms}$ ),  $\varphi$  the efficiency of PF ( $17.1\%$  vs.  $3.7\%$ ), and  $\Phi$  the intersystem crossing efficiency of the sample. Thus, the ratio  $\Phi_{\text{nanosheet}}/\Phi_{\text{bulk}}$  can be estimated to be  $\sim 0.07$ , indicating greatly suppressed ISC efficiency of carbon nitride nanosheets with respect to its bulk counterpart. This result not only echoes to the extremely high PL quantum yield and photocatalytic performance of g-C<sub>3</sub>N<sub>4</sub> nanosheet, but also confirms that the excitonic effect in g-C<sub>3</sub>N<sub>4</sub> matrix serve as a shackle for photocatalytic processes. Note that this is a rough estimation, since the non-classical delayed fluorescence feature of carbon nitride nanosheets.

On the basis of the above analyses, we conclude that carbon nitride nanosheets tend to possess significant suppressed intersystem crossing rate, which lead to low triplet exciton concentration and faint triplet-triplet annihilation, echoing to the extremely high PL quantum yield.

**Table S1.** The fitted fluorescence decay components of g-C<sub>3</sub>N<sub>4</sub> in different solvents.

solvent	$\tau_1$ / ns	$\tau_2$ / ns	$\tau_3$ / ns	Ave. $\tau$ / ns
water	$0.040 \pm 0.001$	$3.63 \pm 0.03$	$11.50 \pm 0.14$	$4.51 \pm 0.05$
	37%	35%	28%	
water/ethanol	$0.037 \pm 0.001$	$2.44 \pm 0.03$	$9.12 \pm 0.12$	$3.24 \pm 0.04$
	39%	35%	26%	
water/2-bromoethanol	$0.038 \pm 0.001$	$0.96 \pm 0.04$	$2.91 \pm 0.15$	$0.50 \pm 0.02$
	62%	22%	9%	

## References

1. X. Zhang, X. Xie, H. Wang, J. Zhang, B. Pan and Y. Xie, *J. Am. Chem. Soc.*, 2013, **135**, 18.
2. S. Yang, Y. Gong, J. Zhang, L. Zhan, L. Ma, Z. Fang, R. Vajtai, X. Wang and P. M. Ajayan, *Adv. Mater.*, 2013, **25**, 2452.
3. Y. Chen, B. Wang, S. Lin, Y. Zhang and X. Wang, *J. Phys. Chem. C*, 2014, **118**, 29981.
4. J. Zhang, Y. Chen and X. Wang, *Energy Environ. Sci.*, 2015, **8**, 3092.
5. D. Beljonne, Z. Shuai, G. Pourtois and J. L. Brédas, *J. Phys. Chem. A*, 2001, **105**, 3899.
6. D. S. McClure, *J. Chem. Phys.*, 1952, **20**, 682.
7. C. A. Parker and T. A. Joyce, *Trans. Faraday Soc.*, 1966 **62**, 2785.
8. C. A. Parker and T. A. Joyce, *Chem. Commun.*, 1966, **185**, 234.